Solid-Core Fiber Spectral Broadening at Its Limits

Marcus Seidel, Xiao Xiao, and Alexander Hartung

***Abstract*—Broadband optical spectra are employed in ultrafast time-resolved studies, seeding of tunable parametric amplifiers, and selectively addressing transitions in absorption spectroscopy. A strong extension of spectral bandwidth is commonly achieved in nonlinear fiber by means of self-phase modulation. In terms of energy scalability and achievable bandwidth, the method is, however, limited by the damage threshold of the core material. Here, we study spectral broadening in four different single-mode normal dispersive photonic crystal fibers length of 8–10 cm. They are pumped by a thin-disk oscillator emitting 250 fs pulses at peak powers close to the critical power of silica. We demonstrate mode-field diameter-dependent broadening factors from 19 to 51, which are obtained at power spectral densities from 200 to 5 mW/nm. We explain the results by a relation between peak power and broadening factor. This will serve as a fiber selection guideline transferable to lasers emitting at wavelengths different from 1030 nm. In addition, we examine to which extend prechirp leads to energy scalability of spectral broadening in solid-core fiber. By contrast to previous reports, we point out that the applicability of the technique is strongly limited through the requirement of bell-shaped input pulses and the pulse duration dependent material damage threshold.**

***Index Terms*—Nonlinear optics, optical fibers, optical pulse compression, solid lasers.**

I. Introduction

SOLID-CORE optical fibers have been utilized since the late 1970s to exploit self-phase modulation (SPM) in order to broaden pulse spectra far beyond the gain bandwidth of active laser media [1]. They enabled, for instance, the generation of the first sub-10 fs pulses in 1985 [2]. With the advent of single-mode photonic crystal fibers (PCFs) [3] and Ti:sapphire oscillators ever broader spectra and shorter pulses were demonstrated [4], approaching the duration of a single carrier wave period [5]. In addition, the waveguides became also attractive for high-power laser architectures with the emergence of large mode area (LMA) fibers [6]. For instance, the first sub-50 fs [7] and the first sub-10 fs pulses [8] derived from the output of mode-locked thin-disk oscillators exploited SPM in solid-core microstructured optical fiber.

The technique is attractive because normal dispersive fibers exhibit good noise and coherence properties [9], [10]. Moreover, large broadening factors can be obtained and good pulse compression can be achieved by compensating only for linear chirp [7], [8]. Furthermore, solid-core fiber broadening at 250 W has been reported [11], demonstrating the capability of good average power handling. Eventually, silica PCFs are widely commercially available and very cost-efficient in comparison to hollow-core PCFs, for example.

Whereas large mode areas have proven to raise the power levels transmittable through solid-core fiber, the trade-off between damage limit and attainable spectral broadening may have been apparent [12], but has not been comprehensively studied to the best of our knowledge. It is therefore instructive to investigate up to which peak power and pulse energy levels, respectively, solid-core fibers present an attractive tool for spectral broadening, especially if optimization of both bandwidth and power is desired. This is particularly interesting for nonlinear applications that require, for instance, ultrashort pulses to resolve fast dynamics of a transition far away from the central laser wavelength, or a large bandwidth to get access to a certain mid-infrared wavelength in difference frequency generation [13].

Here, we investigate the relation between maximal pulse peak power and attainable broadening factor with a Kerr-lens mode-locked thin-disk oscillator which emits pulses with a peak power of 4.6 MW [14], slightly exceeding the critical power of fused silica. We firstly study spectral broadening in PCFs with four different core diameters, and secondly discuss the impact of positive pre-chirp on the power scalability of the technique. We exclude spectral broadening in active fibers [15] from our investigation and restrict the presented study to passive PCFs. With regard to the aforementioned applications, we, moreover, discuss spectral broadening under the premise of temporal compressibility.

II. Mode-Field Diameter Dependent Spectral Broadening Factors and Power Densities

A. Theory

The broadening factor β describes the bandwidth ratio between the self-phase modulated pulses exiting a nonlinear fiber and the initial pulses entering the fiber. It is, for initially unchirped Gaussian pulses and wavelength-independent normal material group velocity disperion (GVD), expressed as the square root of the ratio between nonlinear $\left(L_n = (\gamma P_p)^{-1} = \lambda/(\pi n_2 I_p)\right)$ [16] and dispersion lengths

Manuscript received December 7, 2017; revised January 24, 2018 and February 24, 2018; accepted February 27, 2018. Date of publication March 8, 2018; date of current version March 28, 2018. This work was supported by the Munich-Centre for Advanced Photonics (MAP) under Grant EXC 158 of the Deutsche Forschungsgemeinschaft. The work of A. Hartung was supported by the Federal Ministry of Education and Research (BMBF), funded by the regional alliance Tailored Optical Fibers (Wachstumskern TOF). *(Corresponding author: Marcus Seidel.)*

M. Seidel was with the Max-Planck-Institut für Quantenoptik, Garching, 85748, Germany. He is now with the Institut de Science et d'Ingnierie Supramolculaires (I.S.I.S.), Strasbourg 67000, France (e-mail: seidel@unistra.fr).

X. Xiao was with the Max-Planck-Institut für Quantenoptik, Garching 85748, Germany.

A. Hartung is with the Leibniz-Institute of Photonic Technology, Jena 07745, Germany (e-mail: alexander.hartung@leibniz-ipht.de).

Color versions of one or more of the figures in this paper are available online at http://ieeexplore.ieee.org.

Digital Object Identifier 10.1109/JSTQE.2018.2811907

$\left(L_d = \tau_{in}^2/\mathrm{GVD}\right)$ [17]:

$$\beta = \kappa_1 \sqrt{L_d/L_n} = \kappa_1 \sqrt{\left(\frac{\tau_{in}^2}{\mathrm{GVD}}\right) / \left(\frac{\lambda}{\pi n_2 I_p}\right)} \qquad (1)$$

where κ_1 is a constant, λ denotes the vacuum wavelength, n_0 the linear and n_2 the nonlinear refractive index, τ_{in} the input pulse duration, and I_p the peak irradiance. The use of the nonlinear parameter γ and the peak power P_p is common in the fiber community, but not well suited for the following discussions. The prefactor κ_1 may vary depending on the application. For maximal broadening it is about 0.5, for efficient pulse compression with linear chirp it is about 0.37 [17]. The characteristic lengths also determine the optimal physical fiber length which can be approximated by [17]:

$$L_f = \kappa_2 \sqrt{L_d L_n}, \qquad (2)$$

where the prefactor κ_2 is about 1.4 for efficient pulse compression with linear chirp [17]. As an example, (1) and (2) with $\kappa_1 = 0.37$ and $\kappa_2 = 1.4$ would lead to broadening factors of 16.7 and fiber lengths of 10 cm for the fiber compression experiment presented in [8] where in principle the same setup was used. The estimations are close to the experimental values of 18 and 8 cm, and hence indicate that the simple model can be applied to discuss the scalability of solid-core fiber broadening although it neglects many pulse duration dependent effects like optical breakdown in silica [18]–[20] or the impact of higher-order dispersion and nonlinearities.

Whereas n_2 and the GVD are determined by the fiber material (for large mode areas), λ as well as τ_{in} are given by the light source. Consequently, in order to maximize β, the only free parameter of (1) is the peak irradiance. This motivates investigations of the fiber damage threshold dependence on the mode field diameter (MFD) which determines I_p together with the peak power.

B. Experiment

We examined spectral broadening in four different PCFs (all supplied by NKT photonics): LMA-35, LMA-25, LMA-12 (also referred to as ESM-12) and NL-1050-NEG-1. The LMA fibers exhibit MFDs between 26 and 10 μm as well as the dispersion of fused silica (Fig. 1(b)). The MFD of NL-1050-NEG-1 is only about 3 μm. The small mode area allows to introduce significant waveguide dispersion which was tailored to minimize the GVD near 1050 nm and to keep it positive for all wavelengths [21], [23], [24] (Fig. 1(b)). All fibers were manually cleaved by means of a ruby fiber scribe to avoid micro-cracks on the fiber core surface. Those were usually visible when an automated fiber cleaver was used. Manual cleaving resulted in fiber length variations between 8 and 10 cm which had, however, only a small impact on the broadening factors as Fig. 2 demonstrates. The simulated spectral evolution in a LMA-35 fiber illustrates that the spectral broadening caused by self-phase modulation was saturated and optical wave-breaking into the anomalous dispersion regime was avoided. The latter would complicate pulse compression and significantly enhance intensity noise [25], both being highly detrimental for the aforementioned applications. To

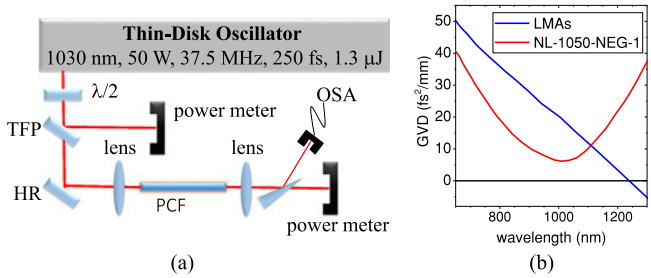

Fig. 1. **(a)** Setup of the solid-core fiber broadening experiments. The input power into the 8–10 cm long PCFs was adjusted with a half-wave plate ($\lambda/2$) and a thin-film polarizer (TFP). HR denotes a highly reflective mirror that steers the beam towards the focusing lens which couples light into the fiber. After collimation, a wedge reflection is sent to an optical spectrum analyzer (OSA). Moreover, the power of the fiber output is monitored behind the wedge. **(b)** Fiber dispersion curve for the LMA fibers (blue solid line, provided by Thorlabs). It corresponds to the GVD of fused silica. The red solid line shows the tailored dispersion of the NL-1050-NEG-1 fiber (from [21]) which is always normal and minimal around 1050 nm.

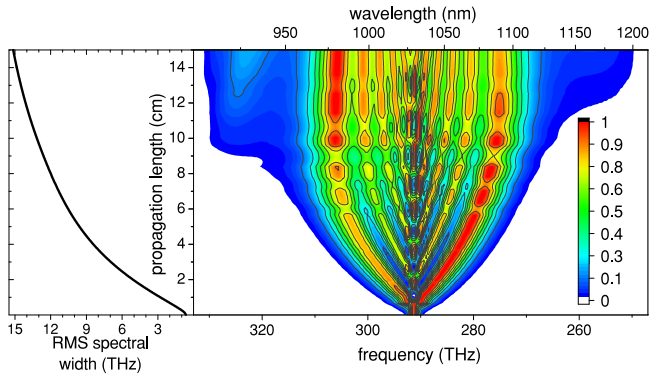

Fig. 2. Simulated spectral evolution of 250 fs, 550 nJ sech^2-pulses propagating through LMA-35 fiber with a MFD of 26 μm. The spectra of the false color plot have been normalized at each propagation length. The modulated part (mainly red, yellow, green colors) of the spectra results from SPM. The effect is saturated after about 8 cm propagation length. At longer propagation length optical wave-breaking becomes the dominant spectral broadening mechanism. The power of the emerging spectral wings remains, however, relatively low (blue colors), and thus the root mean square (RMS) spectral width rises only slowly with propagation length. The simulation has been conducted with fiberdesk V. 2.0 [22]

couple the Gaussian beam emitted from the oscillator to the fundamental fiber mode, lenses with focal lengths f were chosen which approximately sufficed the equation:

$$f = \frac{\pi d_{in} \mathrm{MFD}}{4\lambda}. \qquad (3)$$

The equation refers to the focus size of a Gaussian beam where d_{in} is the diameter of the collimated laser beam before the lens and λ the wavelength. We obtained coupling efficiencies between 65 an 80%, typically higher ones for larger core diameters. The setup is sketched in Fig. 1(a).

Output spectra and transmitted powers were measured while the input power was slowly increased until fiber damage was observed by means of reduced spectral width and transmission. Fig. 3 shows spectra which were measured at input powers slightly below the damage threshold. From the graph, it becomes obvious that smaller MFD lead to broader spectra which

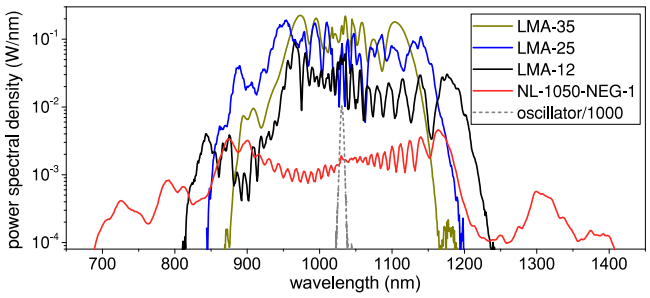

Fig. 3. Exemplary spectra broadened in a PCF and afterwards measured with an optical spectrum analyzer. Four fibers of different MFDs were tested: According to the data sheets provided by NKT photonics, LMA-35 has an MFD of 26.0 μm, LMA-25 of 20.9 μm and LMA-12 of 10.3 μm. The NL-1050-NEG-1 fiber with a tailored waveguide dispersion has an MFD of about 3.0 μm [21]. As a reference, the thin-disk oscillator spectrum is shown as well (gray dashed line). It was measured with a grating spectrometer and is plotted in units of kW/nm.

span over more than one optical octave in the extreme case of the smallest core fiber. Fig. 4(a) displays the broadening factors and the Fourier transform-limits of the measured spectra which were obtained for several fibers of each type within a $\pm$0.5 fs accuracy. For the LMA fibers, Fourier transform-limits between 9 and 13 fs were extracted. The NL-1050-NEG-1 fiber generates spectra with sub-5 fs Fourier transform-limit, resulting in broadening factors of more than 50. In this case, optical wave-breaking had a significant impact on the Fourier transform-limit which requires control of higher-order dispersion for pulse compression as demonstrated in [26]. It is to note, that the use of longer NL-1050-NEG-1 fibers ($\approx$20 cm) and 230 fs input pulses resulted in the generation of incoherent spectra owing to polarization instabilities [27]. These could, however, be circumvented by using the polarization-maintaining version of the fiber [27].

The power measurements revealed that the power spectral density of the smallest core fiber output spectrum does not exceed 5 mW/nm whereas the LMA fibers generate power spectral densities of slightly more than 200 mW/nm at the 37.5 MHz repetition rate of the oscillator. The peak irradiances inside the fibers were calculated from the output power and the MFD which was taken from the data sheets of the LMA fibers and from [21]. We estimated the accuracy to 200 nm for each fiber. For the power measurements, a relative error of 5% was assumed that accounted for the residual transmission of light which was not coupled to the fundamental mode.

The results of Fig. 4(a) and (b) are qualitatively in agreement with the expectations from (1). The gray dashed curve in Fig. 4(a) indicates that the Fourier transform-limits determined after the LMA fibers are close to the $\sqrt{I_p}$ dependence. For a good agreement with the measured broadening factors, κ_1 in (1) was set to 0.45 which is close the values for optimal compression (0.37) and maximal broadening (0.5) [17]. The discrepancy in the broadening factor of the NL-1050-NEG-1 fiber stems from its tailored dispersion entering also (1). Whereas the gray curve in Fig. 4(a), derived from a flat dispersion of 19 fs^2/mm, yields a smaller broadening factor than measured, the actual 3-fold lower GVD at 1030 nm of the NL-1050-NEG-1 fiber would result in a somewhat overestimated broadening factor of 58 due to the non-flat GVD over the optical octave (dark gray triangle in Fig. 4(a)). In simulations, whose results are plotted with a blue dashed curve in Fig. 4(a), the broadening factor of the NL-1050-NEG-1 agrees well with the measured one. Moreover, the $\sqrt{I_p}$ dependence of the broadening factor for the LMA fibers becomes also visible.

The red curves in Fig. 4(b) and (c) show, on the first glance, two rather surprising results: Firstly, although all fibers are made from silica, the calculated peak irradiances strongly differ. The lower the MFD, the higher the peak irradiance the fiber seems to tolerate. Secondly, as expected, the peak powers and pulse energies, respectively, that can be transmitted through the fibers, increase with mode-field diameter. However, even for the largest mode area, the transmittable peak power is still about a factor of two lower than the critical power of fused silica.

C. Origins of Damage

The origins of fiber damage have been described in detail by Smith *et al.* [30]. In general, they arise from instantaneous multi-photon absorptions in combination with free-carrier absorption and electron avalanche, i.e., are caused by strongly irradiance dependent phenomena. Damage is accelerated by (sub-)critical self-focusing which leads to an irradiance enhancement near the fiber and fiber. The behavior is illustrated in Fig. 5. A fixed peak irradiance of 1.3 TW/cm^2 has been assumed at the entrance of a bulk silica sample. Upon varying focus diameter and pulse energy, the impact of self-focusing changes strongly. For large beam diameters, the Gaussian beam divergence is too weak to completely suppress self-focusing. Only after an intermediate focus, diffraction overcomes the nonlinear effect and leads to an expanding beam. For small beam diameters, self-focusing cannot overcome beam diffraction at any propagation length. The observed irradiance enhancement is approximated by [30]:

$$I_{\max}/I_p = (1 - P_p/P_{cr})^{-\kappa_3}, \tag{4}$$

where $I_{\max}$ is the damage threshold and I_p the input irradiance, P_p is the peak and P_{cr} the critical power. The exponent κ_3 depends on the fiber type. For bulk material, it is 1 [30]. This exponent matches best the determined peak irradiances for the LMA fibers. The dashed gray line in Fig. 4(b) shows the peak irradiances corrected with (4), assuming $P_{cr} = 4$ MW [30]. They are (1.55 ± 0.15) TW/cm^2 for the LMA fibers. The peak irradiance in the NL-1050-NEG-1 fiber is with about 2 TW/cm^2 somewhat higher.

To provide additional evidence of sub-critical self-focusing, the fiber front facets were imaged with a light microscope (Fig. 6). Whereas the NL-1050-NEG-1 fiber and LMA-12 exhibit clearly damaged facets, surface modifications are not visible for the larger core fibers. This corresponds to the expectations derived from the enhancement curve of Fig. 5. LMA-25 and LMA-35 could, however, be reused after recleaving, i.e., after removing a few millimeters from the front of the fiber. The observation also implies that collapsing the facets of the small core fibers can in-fact increase the damage threshold. By contrast, collapsing large core fibers may prevent long term

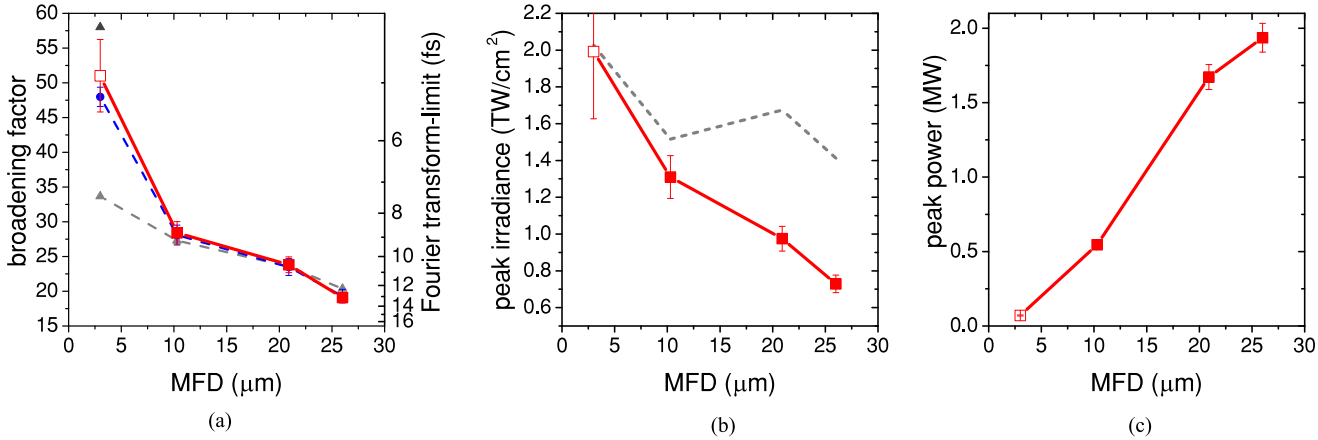

Fig. 4. **(a)** Dependence of the broadening factors and Fourier transform-limits, respectively, on different MFDs of the utilized photonic crystal fibers. Multiple fibers of each type were tested, resulting in a transform-limit uncertainty of ±0.5 fs (red error bars). The dashed gray curve shows the calculated broadening factors derived from (1) inserting the peak irradiances of (b) and $\kappa_1 = 0.45$. The dark gray triangle in the top-left corner represents the calculated broadening factor for GVD = 6.4 fs^2/mm (NL-1050-NEG-1) instead of GVD = 19 fs^2/mm (LMA fibers). The blue dashed line shows simulation results obtained with fiberdesk V. 2.0 [22]. The blue error bars (partly hidden behind the experimental results) show the impact of fiber length variations between 8 cm and 10 cm. **(b)** Peak irradiances derived from the power measurements *behind* the fiber. The red solid curve is predicted from pulse energy, pulse duration and MFD, the gray dashed curve takes into account non-critical self-focusing in the fiber. **(c)** Peak powers tolerated by the fibers. The values were derived from the measured *output* power and the input pulse duration. The hollow red dots in (a)–(c) represent the NL-1050-NEG-1 fiber, the solid red dots the LMA fibers.

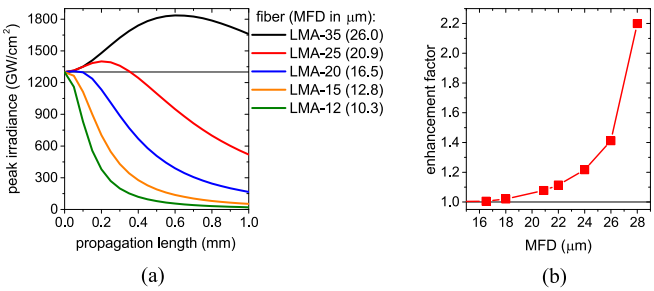

Fig. 5. **(a)** Free beam propagation in 1 mm fused silica is simulated with the SISYFOS code [28], [29]. The peak irradiance is 1.3 TW/cm^2 at the input, the beam size corresponds to the MFD of the commercially available LMA fibers listed in the plot legend. Propagation length 0 is always at the waist of the Gaussian beam. Pulse energies were adapted to the spot sizes in order to keep the irradiance constant. Sub-critical self-focusing becomes apparent for diameters of more than 16.5 μm. **(b)** The enhancement factor, i.e., the ratio between maximal and input irradiance, is plotted over the MFD.

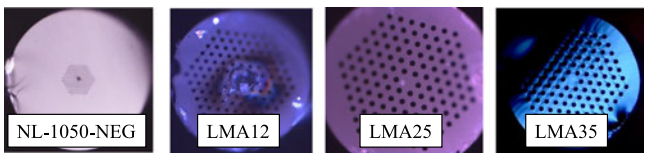

Fig. 6. Microscope images of the front fiber facets after damage. Whereas the core of the NL-1050-NEG-1 and the LMA-12 fibers show severe surface damage, the facets of LMA-25 and LMA-35 do not exhibit modifications.

degradation but does not raise the instantaneous damage threshold. One may use collapsed ends or end caps and correct (3) for the irradiance enhancement when choosing the proper focal length for coupling the free beam to the fiber mode. But, since both the spot size and the focal length change with input power in the sub-critical self-focusing regime, coupling will become very difficult.

The combination of (1) and (4) results in an approximation for a maximal broadening factor:

$$\beta_{\max} \approx \kappa_1 \tau_{in} \sqrt{\left(\frac{\pi n_2 I_{\max}}{\lambda \mathrm{GVD}}\right)\left(1 - \frac{P_p}{P_{cr}}\right)}. \tag{5}$$

The equation presents an implicit guideline for the fiber diameter selection at a given input peak power and for a targeted output bandwidth at maximal power density, respectively. It has been qualitatively verified by the use of several silica PCFs and 250 fs input pulse durations. It can, however, be readily transferred to other input pulse durations and fiber types as long as the assumption of a flat, positive GVD is not strongly violated. It is to point out that $I_{\max}$ depends on the duration of the input pulses [18]–[20], [30] as will be discussed in more detail in the next section.

III. Chirped Pulse Spectral Broadening

A. Concept

The previous paragraphs have described the trade-off between peak power and gain of bandwidth in spectral broadening experiments with normally dispersive PCF. As (5) indicates, the broadening vanishes if the peak power approaches the critical power of the fiber material. Consequently, a first ansatz to achieve low Fourier transform-limits without sacrificing pulse energy is raising the critical power. Jocher *et al.* realized this by using circular instead of linear polarization [11] which increases the critical power by 50% [30]. A second ansatz is to reduce the peak power by increasing the input pulse duration instead of lowering pulse energy. This idea was realized by means of chirping the output of long-cavity Ti:sapphire oscillators which deliver peak powers up to 10 MW [32]. Dombi *et al.* utilized down-chirped pulses to circumvent entrance facet damage of a single-mode fiber with about 5 μm MFD [33]. Ganz *et al.*

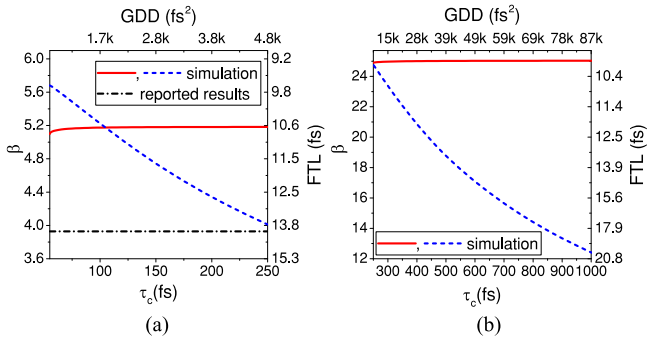

Fig. 7. **(a)** Simulated broadening factors and Fourier transform-limits (FTLs) from the data provided in [31]. Simulations have been performed for a fixed fiber length of $L_f = 3$ cm (as stated in the publication, blue dashed line) and for $L_f = 3\text{ cm} \cdot \tau_c/55$ fs (red solid line). The SISYFOS code was utilized. A temporal grid of 8192 points as well as the full Sellmeier equation of fused silica was used and a plane wave was propagated. For comparison, the reported results from Ganz *et al.* are shown (black dashed line). **(b)** SISYFOS simulations for the LMA-35 experiments presented in [8], predicting the possibility of increasing the pulse energy inversely proportional to the pulse duration (blue dashed line - fixed fiber length of 8 cm, red line - fiber length scales with $\tau_c/250$ fs). The top x-axes show the group delay dispersions which are needed to achieve the pulse durations on the bottom x-axes. These simulations assume a pulse duration *in*dependent damage threshold.

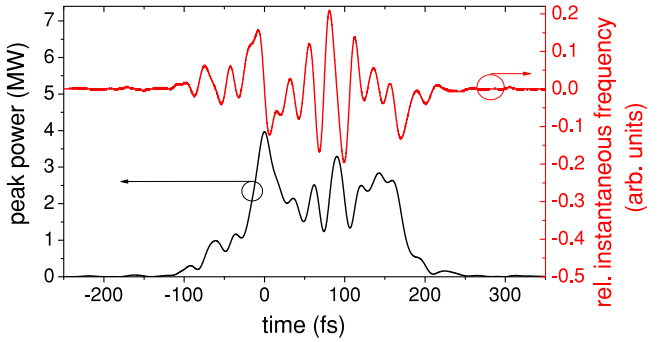

Fig. 8. Pulse after the LMA-35 fiber broadening stage presented in [8] chirped to 4 MW peak power by adding 660 fs^2 group delay dispersion (black solid line). Its numerical time derivative is represented by the red solid line. It shows that the frequencies generated by SPM appear at multiple instances of time which makes good pulse compression impossible. The right axis refers to a relative instantaneous frequency which is superimposed on the frequency sweep introduced by the chirp of the pulse represented by the black line.

increased the pulse duration and energy sent into a LMA-25 fiber compression stage by a factor of four through the usage of up-chirped pulses. Almost the same Fourier transform-limit was reached with both 55 fs nearly transform-limited and longer pre-chirped input pulses. Furthermore, the compression factor was only reduced from 3.8 to 3.4 [31].

Qualitatively speaking, chirping leads to a reduced temporal gradient on the one hand, resulting in a slower spectral broadening. On the other hand, chirp extends the propagation length that is needed to double the pulse duration, and thus also pulse stretching gets slower. Consequently, one may (naively) scale both nonlinear and dispersion length by the ratio between chirped and transform-limited duration τ_c/τ_i, resulting in the same broadening factor according to (1) if, according to (2), the fiber length is also extended by τ_c/τ_i. It is to note that L_n of an transform-limited pulse does not explicitly depend on the pulse duration because both the initial bandwidth and the temporal gradient are proportional to the inverse of the pulse duration. However, if the pulses are chirped, the temporal gradient is reduced whereas the bandwidth remains constant and the τ_c/τ_i-factor arises. In a similar way, it can be argued that the dispersion length does not only depend on the actual pulse duration, but also on the bandwidth. Fig. 7 shows simulation results which demonstrate that these simple considerations theoretically work well. Both for the experiment of [31] and for the pulse parameters of the mode-locked thin-disk oscillator utilized in here, a nearly constant broadening factor is predicted.

B. Restrictions

To the best of our knowledge, the restrictions of the chirped pulse spectral broadening method have not yet been discussed in the literature. A first important requirement for applying the technique is the use bell-shaped input pulses. For instance, adding quadratic phase to a Gaussian changes the pulse duration but not the pulse shape, i.e., the pulses remain Gaussian [17]. This is, however, generally not true for arbitrary spectra. For example, if chirped pulse broadening is employed in a double fiber stage setup, the self-phase modulated spectrum after the first stage will also lead to a strongly modulated pulse shape after applying some chirp. An example is shown in Fig. 8. Here, a compressed pulse after the LMA-35 fiber stage presented in [8] is positively chirped to reduce the peak power below the critical power. Since the instantaneous frequencies which are generated by SPM are proportional to the time derivative of the pulse shape [17], the very same frequencies would have been generated at multiple instances of time (red solid line in Fig. 8(a)). Although four-wave mixing may additionally change the temporal frequency distribution, compression by dispersive optics seems basically impossible.

A second severe restriction results from the pulse duration dependence of the damage threshold. The single pulse studies of Stuart *et al.*, Lenzner *et al.* and Tien *et al.* [18]–[20] show that the damage irradiance of bulk fused silica scales approximately with $\tau^{-3/4}$ for sub-10 ps pulses where the dominant, non-instantaneous impact ionization has not fully evolved. Smith *et al.* argue that fiber damage underlies the same physical mechanisms [30]. Although long living trap states decrease the damage threshold if multiple pulses are incident [34], it is not expected that the electron avalanche is accelerated. Upon taking into account (4), the peak irradiance in the fiber is calculated by:

$$I_p = I_{\max,i}\left(\frac{\tau_i}{\tau_c}\right)^{3/4}\left(1 - \frac{P_{p,i}}{P_{cr}}\frac{\tau_i}{\tau_c}\right), \tag{6}$$

where $I_{\max,i}$ and $P_{p,i}$ are the damage irradiance and the peak power of the transform-limited pulses.

Two examples applying (6) are shown in Fig. 9. In (a), the peak power of a transform-limited pulse is set to 2 MW, half of the critical power. With regard to the results of Sections II and III-A, pre-chirp could be expected to increase the broadening factor without sacrificing pulse energy. The graph demonstrates,

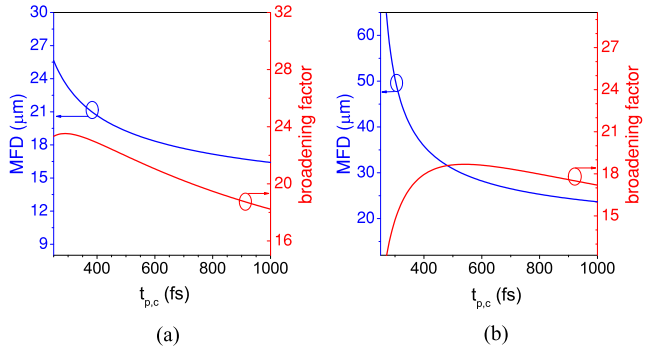

Fig. 9. MFDs and broadening factors for various input pulse durations τ_c derived from (1) and (6) where $\tau_i = 250$ fs, GVD= 19 fs^2/mm, $\lambda = 1030$ nm, $n_2 = 2.8 \cdot 10^{-16}$ cm^2/W, $P_{cr} = 4$ MW and $\kappa_1 = 0.5$. **(a)** An initial peak power of $P_{p,i} \approx 2$ MW is set. Pre-chirping hardly increases the maximum broadening factor if the damage irradiance scales $\propto \tau^{-3/4}$. **(b)** An initial peak power of $P_{p,i} \approx 4$ MW is set, being close to the critical power. In this case, an optimal chirp and MFD can be derived, indicating possible applicability of chirped pulse spectral broadening.

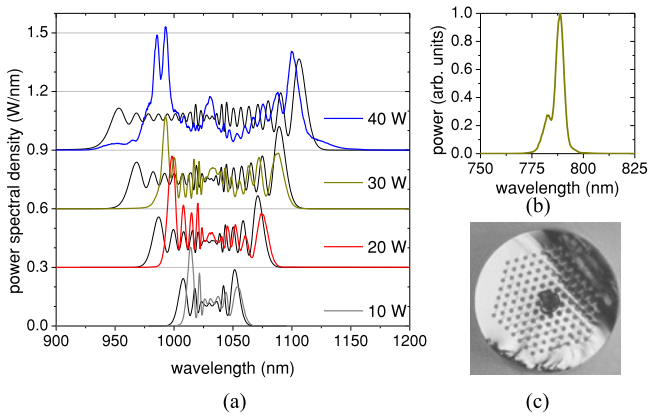

Fig. 10. **(a)** Measured chirped pulse spectra after ≈12 cm propagation in LMA-25 (gray, red, dark yellow, blue thicker solid lines) and comparison to spectra simulated with fiberdesk V. 2.0 (black solid lines) at different input power levels. For visibility the spectra are offset by 0.3 W/nm. **(b)** Spectrum of a feature appearing on the anti-Stokes side for input powers of at least 30 W. **(c)** Fiber front facet after damage at 43 W input power. Contrary to the LMA-25 facet in Fig. 6, the surface is clearly disrupted.

however, that chirped pulse spectral broadening is not applicable in this case. By contrast, upon doubling $P_{p,i}$ to about 4 MW, which corresponds to the output of the utilized mode-locked thin-disk oscillator, an ideal input pulse duration between 500 and 600 fs is predicted (Fig 9(b)). The expected broadening factor is about 18.7 which is 17% lower than what has been predicted for LMA-35 by means of (1), but the transmitted peak power would double.

C. Example

An experiment utilizing 590 fs pulses was conducted. The 250 fs pulses emerging from the mode-locked thin-disk oscillator were chirped by 24 bounces off chirped mirrors with +2000 fs^2 group delay dispersion per bounce. The stretcher consisted of 8 chirped mirror pairs and a recollimation mirror with 1 m focal length. An about 12 cm long LMA-25 fiber was tested. An average power of 45.5 W was available after the stretcher. Damage occurred at 43 W input power. Consequently, about 60% more pulse energy was transmitted through the fiber, whereas the peak power was reduced by approximately 30% to 1.3 MW. Taking into account the enhancement factor of (4), the damage irradiance was reduced to 66% of the unchirped value. For comparison, the theoretical value, assuming the scaling of (6), would be 53%. The reduced irradiance enhancement was evidenced by the fiber facet of the damaged LMA-25, shown in Fig. 10(b). In contrast to the facet of Fig. 6, it exhibits very clear signs of destruction.

Fig. 10(a) shows the spectra measured behind the fiber at four different power levels and corresponding simulations. Although at up to 30 W input power the spectral broadening is overestimated in the simulations, the spectral shape qualitatively agrees in the sense that the central spectral modulations are reduced in comparison to the measurements with transform-limited pulses and optical wave-breaking is suppressed. This results from the pre-chirp and the corresponding increased temporal stretching of the instantaneous frequencies generated through SPM [16]. The spectrum at 40 W input power is qualitatively different. Although its Fourier transform-limit of about 16 fs is in good agreement with the simulated spectrum, spectral side-lobes appear in the experiment that have not been computed. Furthermore, relatively narrow spectral lines on the anti-Stokes side at 790 nm and 660 nm central wavelengths appeared together with a visible red glowing of the fiber after increasing the input average power to more than 30 W (cf. Fig. 10(b)). Such spurious nonlinearities have not been observed for any of the measurements discussed in Section II. They present an additional loss channel which is further reducing the peak power enhancement attainable with chirped pulse spectral broadening. We would like to note that the detected anti-Stokes lines have neither been predicted in fiberdesk nor SISYFOS simulations modeling the Raman response as proposed in [16]. The increase of both input pulse duration and fiber length leads to an enhanced Raman gain inside the fiber [10] and we suspect this to cause the additional spectral feature which was not observed in the experiments with Fourier transform-limited pulses. As the side-lobes shown in Fig. 10(a) for 40 W input power do not arise from SPM, the compression down to the 16 fs Fourier transform-limit is expected to be also more complicated than the compression of the LMA spectra shown in Fig. 3.

IV. Summary

In summary, we have demonstrated that chirped pulse broadening is not as general as claimed in its initial publication [31]. Apart from the time-dependent damage threshold, it appears restricted to bell-shaped pulses where chirp hardly changes the pulse shape. Furthermore, parasitic nonlinear effects were observed in the experiment with 590 fs pulses which present an additional source of peak power reduction. Therefore, the method appears to be quite restricted to lasers with peak powers slightly above the critical power of the fiber material, like long-cavity Ti:sapphire oscillators [32]. Consequently, pulse compression schemes based on bulk materials [37]–[40] or hollow-core

TABLE I
CRITICAL POWERS OF MULTIPLE FIBER MATERIALS[a]

type	silica	fluoride	tellurite	chalcogenide
material	SiO_2	ZBLAN	$ZnO\text{-}Te_2$	As_2S_3
λ_0^b	1.26 μm	1.62 μm	2.24 μm	4.81 μm
P_{cr} (1 μm)	4 MW	3 MW	150 kW	10 kW
P_{cr} (λ_0)	6 MW	8 MW	700 kW	200 kW

[a] Calculated by $P_{cr} \approx 0.0148\lambda^2/n_0/n_2$ [30]. Refractive indices taken from [35], see also [36]. Dispersion is neglected.
[b] Values for zero-dispersion wavelengths λ_0 taken from [35]

photonic crystal fibers [41], [42] appear clearly superior for femtosecond sources with several μJ of pulse energies.

Nevertheless, there are multiple applications of solid-core spectral broadening where the results presented here can be employed. For instance, we utilized the study presented in Section II in order to choose an appropriate seed source for mid-infrared generation via optical parametric amplification [43]. Furthermore, high power (near-) GHz repetition rate lasers [44], being particularly attractive for frequency comb spectroscopy, will emit only sub-μJ pulses. They can exploit the relations derived here in order to generate large bandwidths. In addition, spectral broadening in PCFs has been recently demonstrated as tool for multi-photon microscopy [45]. Our results can be utilized in order to maximize spectral power densities at the wavelength used for imaging. Finally, the discussions on the relations between peak power, peak irradiance, broadening factor and choice of the MFD may not only be applicable to high average power near-IR lasers, but also to lower average power light sources in combination with fiber materials of higher nonlinearity. Table I presents critical powers of several materials employed in fiber-based spectral broadening schemes. Whereas fused silica is best suited for the utilized thin-disk oscillator, the other materials are particularly attractive for spectral broadening in the mid-infrared [36].

In conclusion, our findings, relating the origins of fiber damage to the maximal broadening factor resulting mainly from SPM, will have impact on spectral broadening experiments with state-of-the art commercial ultrafast solid-state oscillators and fiber amplifiers as well as on newly evolving high repetition rate sources in the short wavelength mid-infrared. The discussion of pulse shape and pulse duration dependent adverse effects in chirped pulse broadening clearer defines the applicability of the method and demonstrates that the trade-off between transmittable pulse energy and obtainable spectral bandwidth can generally not be fully overcome in nonlinear fiber stages.

ACKNOWLEDGMENT

The authors would like to thank many colleagues at MPQ for fruitful discussions, namely: P. Baum, L. Lötscher, A. Apolonski, N. Lilienfein, O. Pronin, and F. Krausz. They would also like to thank V. Pervak for providing the chirped mirrors and G. Arisholm for extending the SISYFOS package to applications to pulse propagation in nonlinear fiber.

REFERENCES

[1] R. H. Stolen and C. Lin, "Self-phase-modulation in silica optical fibers," *Phys. Rev. A*, vol. 17, pp. 1448–1453, Apr. 1978.
[2] W. H. Knox *et al.*, "Optical pulse compression to 8 fs at a 5 kHz repetition rate," *Appl. Phys. Lett.*, vol. 46, no. 12, pp. 1120–1121, 1985.
[3] T. A. Birks, J. C. Knight, and P. S. Russell, "Endlessly single-mode photonic crystal fiber," *Opt. Lett.*, vol. 22, no. 13, pp. 961–963, 1997.
[4] B. Schenkel, R. Paschotta, and U. Keller, "Pulse compression with supercontinuum generation in microstructure fibers," *J. Opt. Soc. Amer. B*, vol. 22, no. 3, pp. 687–693, Mar. 2005.
[5] S. Demmler *et al.*, "Generation of high quality, 1.3 cycle pulses by active phase control of an octave spanning supercontinuum," *Opt. Express*, vol. 19, no. 21, pp. 20 151–20 158, Oct. 2011.
[6] J. Knight, T. Birks, R. Cregan, P. Russell, and J.-P. de Sandro, "Large mode area photonic crystal fibre," *Electron. Lett.*, vol. 34, no. 13, pp. 1347–1348, 1998.
[7] T. Südmeyer *et al.*, "Nonlinear femtosecond pulse compression at high average power levels by use of a large-mode-area holey fiber," *Opt. Lett.*, vol. 28, no. 20, pp. 1951–1953, Oct. 2003.
[8] O. Pronin *et al.*, "High-power multi-megahertz source of waveform-stabilized few-cycle light," *Nature Commun.*, vol. 6, May 2015, Art no. 6988.
[9] J. M. Dudley, G. Genty, and S. Coen, "Supercontinuum generation in photonic crystal fiber," *Rev. Mod. Phys.*, vol. 78, pp. 1135–1184, Oct. 2006.
[10] R. R. Alfano, Ed., *The Supercontinuum Laser Source*. New York, NY, USA: Springer, 2016.
[11] C. Jocher, T. Eidam, S. Hädrich, J. Limpert, and A. Tünnermann, "Sub 25 fs pulses from solid-core nonlinear compression stage at 250 W of average power," *Opt. Lett.*, vol. 37, no. 21, pp. 4407–4409, Nov. 2012.
[12] J. Fekete, P. Rácz, and P. Dombi, "Compression of long-cavity Ti: Sapphire oscillator pulses with large-mode-area photonic crystal fibers," *Appl. Phys. B*, vol. 111, no. 3, pp. 415–418, May 2013.
[13] I. Pupeza *et al.*, "High-power sub-two-cycle mid-infrared pulses at 100 MHz repetition rate," *Nature Photon.*, vol. 9, no. 11, pp. 721–724, Nov. 2015.
[14] O. Pronin *et al.*, "High-power 200 fs Kerr-lens mode-locked Yb: YAG thin-disk oscillator," *Opt. Lett.*, vol. 36, no. 24, pp. 4746–4748, Dec. 2011.
[15] C. J. Saraceno, O. H. Heckl, C. R. E. Baer, T. Südmeyer, and U. Keller, "Pulse compression of a high-power thin disk laser using rod-type fiber amplifiers," *Opt. Express*, vol. 19, no. 2, pp. 1395–1407, Jan. 2011.
[16] G. Agrawal, Ed., *Nonlinear Fiber Optics*, 5th ed. Boston, MA, USA: Academic, 2013.
[17] J.-C. Diels and W. Rudolph, *Ultrashort Laser Pulse Phenomena*, 2nd ed. Burlington, NJ, USA: Academic, 2006.
[18] B. C. Stuart, M. D. Feit, A. M. Rubenchik, B. W. Shore, and M. D. Perry, "Laser-induced damage in dielectrics with nanosecond to subpicosecond pulses," *Phys. Rev. Lett.*, vol. 74, pp. 2248–2251, Mar. 1995.
[19] M. Lenzner *et al.*, "Femtosecond optical breakdown in dielectrics," *Phys. Rev. Lett.*, vol. 80, pp. 4076–4079, May 1998.
[20] A.-C. Tien, S. Backus, H. Kapteyn, M. Murnane, and G. Mourou, "Short-pulse laser damage in transparent materials as a function of pulse duration," *Phys. Rev. Lett.*, vol. 82, pp. 3883–3886, May 1999.
[21] A. M. Heidt *et al.*, "Coherent octave spanning near-infrared and visible supercontinuum generation in all-normal dispersion photonic crystal fibers," *Opt. Express*, vol. 19, no. 4, pp. 3775–3787, Feb. 2011.
[22] Fiberdesk Nonlinear Pulse Propagation. [Online]. Available: https://www.fiberdesk.com/. Version 2 (2007).
[23] A. M. Heidt, "Pulse preserving flat-top supercontinuum generation in all-normal dispersion photonic crystal fibers," *J. Opt. Soc. Amer. B*, vol. 27, no. 3, pp. 550–559, Mar. 2010.
[24] L. E. Hooper, P. J. Mosley, A. C. Muir, W. J. Wadsworth, and J. C. Knight, "Coherent supercontinuum generation in photonic crystal fiber with all-normal group velocity dispersion," *Opt. Express*, vol. 19, no. 6, pp. 4902–4907, Mar. 2011.
[25] U. Møller and O. Bang, "Intensity noise in normal-pumped picosecond supercontinuum generation, where higher-order raman lines cross into anomalous dispersion regime," *Electron. Lett.*, vol. 49, no. 1, pp. 63–65, Jan. 2013.
[26] Y. Liu, H. Tu, and S. A. Boppart, "Wave-breaking-extended fiber supercontinuum generation for high compression ratio transform-limited pulse compression," *Opt. Lett.*, vol. 37, no. 12, pp. 2172–2174, Jun. 2012.
[27] Y. Liu *et al.*, "Suppressing short-term polarization noise and related spectral decoherence in all-normal dispersion fiber supercontinuum generation," *J. Lightw. Technol* ., vol. 33, no. 9, pp. 1814–1820, May 2015.

[28] G. Arisholm, "General numerical methods for simulating second-order nonlinear interactions in birefringent media," *J. Opt. Soc. Amer. B*, vol. 14, no. 10, pp. 2543–2549, Oct. 1997.
[29] G. Arisholm and H. Fonnum, Simulation System For Optical Science (SISYFOS) Tutorial. 2012. [Online]. Available: http://www.ffi.no/no/Rapporter/12-02042.pdf
[30] A. V. Smith, B. Do, G. Hadley, and R. L. Farrow, "Optical damage limits to pulse energy from fibers," *IEEE J. Sel. Topics Quantum Electron.*, vol. 15, no. 1, pp. 153–158, Jan. 2009.
[31] T. Ganz, V. Pervak, A. Apolonski, and P. Baum, "16 fs, 350 nJ pulses at 5 MHz repetition rate delivered by chirped pulse compression in fibers," *Opt. Lett.*, vol. 36, no. 7, pp. 1107–1109, Apr. 2011.
[32] S. Naumov *et al.*, "Approaching the microjoule frontier with femtosecond laser oscillators," *New J. Phys.*, vol. 7, no. 1, 2005, Art. no. 216.
[33] P. Dombi, P. Antal, J. Fekete, R. Szipőcs, and Z. Várallyay, "Chirped-pulse supercontinuum generation with a long-cavity Ti: Sapphire oscillator," *Appl. Phys. B*, vol. 88, no. 3, pp. 379–384, Aug. 2007.
[34] M. Mero *et al.*, "On the damage behavior of dielectric films when illuminated with multiple femtosecond laser pulses," *Opt. Eng.*, vol. 44, no. 5, 2005, Art. no. 051 107.
[35] J. Dudley and J. Taylor, Eds., *Supercontinuum Generation in Optical Fibers*. Cambridge U.K.: Cambridge Univ. Press, 2010.
[36] J. Swiderski, "High-power mid-infrared supercontinuum sources: Current status and future perspectives," *Progress Quantum Electron.*, vol. 38, no. 5, pp. 189–235, 2014.
[37] M. Seidel, G. Arisholm, J. Brons, V. Pervak, and O. Pronin, "All solid-state spectral broadening: An average and peak power scalable method for compression of ultrashort pulses," *Opt. Express*, vol. 24, no. 9, pp. 9412–9428, May 2016.
[38] J. Schulte, T. Sartorius, J. Weitenberg, A. Vernaleken, and P. Russbueldt, "Nonlinear pulse compression in a multi-pass cell," *Opt. Lett.*, vol. 41, no. 19, pp. 4511–4514, Oct. 2016.
[39] M. Seidel *et al.*, "Efficient high-power ultrashort pulse compression in self-defocusing bulk media," *Sci. Rep.*, vol. 7, no. 1, 2017, Art no. 1410.
[40] J. Weitenberg *et al.*, "Multi-pass-cell-based nonlinear pulse compression to 115 fs at 7.5 μJ pulse energy and 300 W average power," *Opt. Express*, vol. 25, no. 17, pp. 20 502–20 510, Aug. 2017.
[41] F. Emaury *et al.*, "Efficient spectral broadening in the 100-W average power regime using gas-filled kagome HC-PCF and pulse compression," *Opt. Lett.*, vol. 39, no. 24, pp. 6843–6846, Dec. 2014.
[42] K. F. Mak *et al.*, "Compressing μJ-level pulses from 250 fs to sub-10 fs at 38-MHz repetition rate using two gas-filled hollow-core photonic crystal fiber stages," *Opt. Lett.*, vol. 40, no. 7, pp. 1238–1241, Apr. 2015.
[43] M. Seidel *et al.*, "Multi-Watt, multi-octave, mid-infrared femtosecond source," *Sci. Adv.*, 4 eaaq1526 (2018).
[44] J. Zhang *et al.*, "260-megahertz, megawatt-level thin-disk oscillator," *Opt. Lett.*, vol. 40, no. 8, pp. 1627–1630, Apr. 2015.
[45] W. Liu *et al.*, "Energetic ultrafast fiber laser sources tunable in 1030–1215 nm for deep tissue multi-photon microscopy," *Opt. Express*, vol. 25, no. 6, pp. 6822–6831, Mar. 2017.

Marcus Seidel was born in Marienberg, Germany, in 1986. He received the Diploma degree in physics from the Free University of Berlin, Berlin, Germany, and the University of Rostock, Rostock, Germany, in 2012, and the M.Sc. degree in optics and photonics from the University of Central Florida, Orlando, FL, USA, in 2011. From 2012 to 2017, he conducted the Ph.D. work at the Max-Planck Institute of Quantum Optics, Garching, Germany.

Since mid of 2017, he has been with the Nanostructures Laboratory, Institut de Science et d'Ingnierie Supramolculaires, Strasbourg, France. His current research interests include ultrashort pulse compression, the development of high-power femtosecond mid-infrared sources, and strong coupling of vibrational transitions to optical cavity modes.

Mr. Seidel is a member of the Deutsche Physikalische Gesellschaft. He received a Fulbright fellowship in 2010, a fellowship of the German Academic Scholarship Foundation in 2012, a Marie Skłodowska-Curie fellowship (European Commission) in 2017, and the Tingye Li Innovation Prize (Optical Society of America Foundation) in 2016.

Xiao Xiao was born in Qinhuangdao, China, in 1991. He received the B.S. degree in optics from Tianjin University, Tianjin, China, in 2013 and the M.Sc. degree in physics from Technical University Munich, Munich, Germany, in 2017.

As a Master's student, he was with the Max-Planck Institute of Quantum Optics, Garching, Germany. His research areas include optical parametric amplifiers, super-continuum generation and pulse broadening and compression.

Alexander Hartung was born in Heiligenstadt, Germany, in 1982. He received the Diploma degree in physics from Friedrich-Schiller-Universitt Jena, Jena, Germany, in 2007.

Since 2007, he has been a Scientist with the Fiber Optics Department, Leibniz Institute of Photonic Technology, Jena, Germany, where he finished the doctoral studies focused on nonlinear pulse propagation and supercontinuum generation in 2012. His research interests include nonlinear pulse propagation, fiber Bragg grating applications in sensors and fiber lasers, and hollow-core optical waveguides.